Durairaj, Vasuki; Liljeström, Touko; Wester, Niklas; Engelhardt, Peter; Sainio, Sami; Wilson, Benjamin P.; Li, Panpan; Kontturi, Katri S.; Tammelin, Tekla; Laurila, Tomi; Koskinen, Jari

Role of nanocellulose in tailoring electroanalytical performance of hybrid nanocellulose/multiwalled carbon nanotube electrodes

Published in:
Cellulose

DOI:
10.1007/s10570-022-04836-8

Published: 01/11/2022

Document Version
Publisher's PDF, also known as Version of record

Cellulose (2022) 29:9217–9233
https://doi.org/10.1007/s10570-022-04836-8

ORIGINAL RESEARCH

Role of nanocellulose in tailoring electroanalytical performance of hybrid nanocellulose/multiwalled carbon nanotube electrodes

Vasuki Durairaj · Touko Liljeström · Niklas Wester · Peter Engelhardt · Sami Sainio · Benjamin P. Wilson · Panpan Li · Katri S. Kontturi · Tekla Tammelin · Tomi Laurila · Jari Koskinen

Received: 15 June 2022 / Accepted: 4 September 2022 / Published online: 15 September 2022

Abstract Nanocellulose has emerged as a promising green dispersant for carbon nanotubes (CNTs), and there is an increasing trend in developing nanocellulose/CNT hybrid materials for electrochemical detection of various small molecules. However, there have been very few comprehensive studies investigating the role of nanocellulosic material properties upon the electroanalytical performance of the resultant hybrid electrodes. In this work, we demonstrate the influence of both nanocellulose functionalization and geometry, utilizing sulfated cellulose nanocrystals, sulfated cellulose nanofibers, and TEMPO-oxidized cellulose nanofibers. Transmission electron microscopy tomography enables direct visualization of the effect of nanocellulosic materials on the hybrid architectures. High resolution X-ray absorption spectroscopy verifies that the chemical nature of CNTs in the different hybrids is unmodified. Electroanalytical performances of the different nanocellulose/CNT hybrid electrodes are critically evaluated using physiologically relevant biomolecules with different charge such as, dopamine (cationic), paracetamol (neutral), and uric acid (anionic). The hybrid

Supplementary Information The online version contains supplementary material available at https://doi.org/10.1007/s10570-022-04836-8.

V. Durairaj (✉) · T. Liljeström · N. Wester · T. Laurila · J. Koskinen
Department of Chemistry and Materials Science, School of Chemical Engineering, Aalto University, P.O. Box 16100, 00076 Aalto, Finland
e-mail: vasuki.durairaj@aalto.fi

P. Engelhardt
Department of Applied Physics, School of Science, Aalto University, P.O. Box 15100, 00076 Aalto, Finland

S. Sainio
SLAC National Accelerator Laboratory, Stanford Synchrotron Radiation Lightsource, Menlo Park, CA 94025, USA

S. Sainio
Microelectronics Research Unit, Faculty of Information Technology and Electrical Engineering, University of Oulu, PO Box 4500, 90570 Oulu, Finland

B. P. Wilson
Department of Chemical and Metallurgical Engineering, School of Chemical Engineering, Aalto University, P.O. Box 16200, 00076 Aalto, Finland

P. Li · K. S. Kontturi · T. Tammelin
Sustainable Products and Materials, VTT Technical Research Centre of Finland, P.O. Box 1000, 02044 Espoo, Finland

T. Laurila
Department of Electrical Engineering and Automation, School of Electrical Engineering, Aalto University, PO Box 13500, 00076 Aalto, Finland

electrode containing fibrillar nanocellulose geometry with a high degree of sulfate group functionalization provides the highest electroanalytical sensitivity and strongest enrichment towards all studied analytes. These results clearly demonstrate for the first time, the extent of tailorability upon the electroanalytical response of nanocellulose/CNT hybrid electrodes towards different biomolecules, offered simply by the choice of nanocellulosic materials.

Keywords Nanocellulose · Carbon nanotubes · Hybrid materials · Electrochemical

Introduction

Cellulose, being the most abundant bio polymer on the planet, offers a sustainable alternative to petroleum-based synthetic polymers in various applications ranging from packaging to biotechnology. The successful extraction of nanoscale structures from plant-based cellulosic materials (Tang et al. 2022; Desmaisons et al. 2017) has further augmented their applicability in the development of various high-value functional hybrid materials (Zhang et al. 2013; Heise et al. 2021; Kontturi et al. 2018; Ferreira et al. 2020). Plant-based nanocellulosic materials can be primarily classified into cellulose nanocrystals (CNCs) composed of predominantly highly crystalline regions of cellulose units, and cellulose nanofibrils (CNFs) containing both crystalline and disordered regions (Abdul Khalil et al. 2014; Tang et al. 2022; Kontturi et al. 2018). The dimensions and surface chemistry of the nanocellulosic materials are heavily dependent upon their plant source as well as the type of mechanical and chemical extraction processes used (Abu-Danso et al. 2017; Habibi et al. 2010). In addition, the highly reactive surface hydroxyl groups on the cellulose units can be further functionalized using several different chemical reactions (Habibi 2014; Eyley and Thielemans 2014). The increasing research interests and capabilities in production and functionalization, have thus led to the availability of a highly versatile set of nanocellulosic materials for various applications.

Malho et al. (2012) demonstrated for the first time that aqueous suspensions of CNFs can be used to directly exfoliate graphene flakes without the need for any further additives. Soon after, Olivier et al. (2012) demonstrated that single walled carbon nanotubes (SWCNTs) can be similarly dispersed in CNC colloidal suspensions. This led to an exponential increase in the research of nanocellulosic materials as environmentally and economically friendly, green alternatives for the dispersion of carbon nanomaterials, aimed at the development of functional hybrid materials for applications such as flexible electronics, energy storage and electrochemical sensing (Hamedi et al. 2014; Li et al. 2015; Hajian et al. 2017; Wang et al. 2020). Carbon nanomaterials are highly attractive for electrochemical sensing applications owing to their unique properties such as large active surface area, high chemical inertness, excellent mechanical strength, low charge transfer resistance and wide operation potential (Merkoçi et al. 2005; Lawal 2016; Papakonstantinou et al. 2005; Primo et al. 2013; Jacobs et al. 2010; Vashist et al. 2011). In particular, multiwalled carbon nanotubes (MWCNTs), present several advantages such as lower production costs, high yield, and robustness when subject to different functionalization processes, thereby making them a more commercially viable option for large scale production of electrochemical sensors (Oliveira and Morais 2018).

A major hurdle in the path to industrialization of MWCNT-based electroanalytical devices remains to be the stable dispersion of MWCNTs for electrode fabrication without the loss of effective electrochemical area and functionality (Rastogi et al. 2008). The large aspect ratios and strong π–π interactions lead to inherent bundling and entanglement of MWCNTs, thereby resulting in their poor dispersibility in both aqueous and non-aqueous media (Chang et al. 2015). Over the years several chemical (covalent) (Fatin et al. 2014; Osorio et al. 2008) and mechanical (non-covalent) (Li et al. 2009; Tong et al. 2010; Yu et al. 2007) methods have been proposed to improve the dispersion of MWCNTs in various matrices. Nanocellulosic materials possess several unique advantages as dispersants of MWCNTs for electroanalytical applications. Their inherent hygroscopicity can improve the wettability of MWCNTs in the hybrid architectures, thereby improving time response and selectivity compared to other hydrophobic polymer dispersants (Durairaj et al. 2019). Further, their large surface area with potential for functionalization can be used to tailor ionic conductivity and improve selectivity of the

hybrid nanocellulose/MWCNT electrodes towards specific biomolecules.

Although several promising electrochemical applications of nanocellulose/nanocarbon hybrid materials are being proposed in the recent years (Muguruma et al. 2016; Shalauddin et al. 2019; Ortolani et al. 2019; Zaid et al. 2020; Shahrokhian et al. 2015), there are not many systematic studies investigating the effects of using different nanocellulose grades upon the observed electrochemical performance. Very recently, Dortez et al. (2022) reported the effect of different polymorphs of CNCs (cellulose I and II), upon the electroanalytical performance of their hybrids with SWCNTs, for detecting glycoproteins. They reported that the cellulose II based hybrid exhibited a higher sensitivity, likely due to a more macroporous structure. In our previous work (Durairaj et al. 2021), we demonstrated that both CNCs and CNFs, functionalized with different surface chemistries, are capable of producing highly stable aqueous suspensions of commercial MWCNTs without the need for any prior purification or chemical modification of the MWCNTs and the nanocellulose/MWCNT suspensions can be used to produce highly stable and repeatable electrochemical platforms with a wide operation potential (– 0.6 to + 1 V), suitable for electroanalytical applications. Investigations with outer sphere redox (OSR) probes indicated that both morphological and electrostatic effects, resulting from nanocellulose geometry and functionalization, play a dominant role in the electrochemical response of the hybrid, and that these differences are further dependent on the ionic strength of the supporting electrolyte.

Such observations emphasize the need for thorough characterizations of the physical and chemical nature of such materials and their correlation to the electroanalytical performance. Most analytes of practical interest are inner sphere redox (ISR) molecules, whose electrochemical responses are highly dependent on the physical and chemical properties of the active electrode surface, and cannot be extrapolated from studies with OSR probes alone. Therefore, this study focuses on evaluating the electrochemical behavior of different nanocellulose/MWCNT hybrid materials towards a carefully selected group of probe molecules, namely dopamine (DA), paracetamol (PA) and uric acid (UA), using cyclic voltammetry (CV) measurements. Two prevalent nanocellulose grades, namely sulfated cellulose nanocrystals (SCNCs) and TEMPO (2,2,6,6-tetramethylpiperidin-1-oxyl)-mediated oxidized cellulose nanofibrils (TOCNFs), are chosen along with reference sulfated cellulose nanofibrils (SCNFs), in order to investigate the effects of both nanocellulose geometry (SCNC vs. SCNF), and functional group (SCNF vs. TOCNF). A transmission electron microscope (TEM) tomography technique is employed to obtain three-dimensional reconstructions of the different nanocellulose/MWCNT hybrid materials, in order to provide a better visual understanding of the network architectures resulting from the dispersion of MWCNTs by different nanocellulosic materials. Surface carbon and oxygen-based functionalities of the MWCNTs in the hybrid materials with different nanocellulosic materials are investigated using X-ray absorption spectroscopy (XAS), to identify any changes in the electrochemically active surface of the MWCNTs. Cyclic voltammetry (CV) measurements at different scan rates, together with enrichment and washout studies, provide useful insights on the role of nanocellulose in determining the electroanalytical performance of the hybrid materials towards different biomolecules.

Experimental

Preparation of nanocellulose/MWCNT suspensions

Preparation and characterization of the different functionalized nanocellulosic materials (SCNCs, SCNFs and TOCNFs) are described in detail in the previous work (Durairaj et al. 2021). In brief, (1) SCNCs were prepared by sulfuric acid hydrolysis of cotton cellulose paper (Dong et al. 1998; Niinivaara et al. 2016), (2) SCNFs were prepared by direct sulfation of softwood dissolving cellulose pulp using a deep eutectic solvent (DES) mixture of sulfamic acid and urea (Sirviö et al. 2019; Li et al. 2019), and (3) TOCNFs were prepared by TEMPO-mediated oxidation of bleached birch pulp (Saito et al. 2007; Isogai et al. 2011). The degrees of different functional group substitutions were determined to be 0.17 mmol/g [OSO_3^-] for SCNCs, 1.7 mmol/g [OSO_3^-] for SCNFs and 1.3 mmol/g [COO^-] for TOCNFs, respectively (Durairaj et al. 2021). Commercial MWCNTs, produced by chemical vapor deposition (CVD) using iron catalysts, were purchased from NanoLab, Inc. (Newton, MA). Aqueous nanocellulose suspensions

were first diluted to 0.25 wt% and 0.125 g of commercial MWCNTs in dry powder form (as obtained, not functionalized) was added to 10 g of each functionalized nanocellulose suspension, such that the final dry weight percentages were 2:1 (Nanocellulose : MWCNTs). The nanocellulose/MWCNT mixtures were tip sonicated in an ice bath, using a Qsonica Q500 tip sonicator, with a 2 mm probe at 20 kHz (30 W), for 10 min in pulsed mode (5 s on and 1 s off). The dispersion quality was assessed by UV–visible spectroscopy (details published previously Durairaj et al. 2021). The dispersions have been kept in a refrigerator at 5 °C and have been found to be stable based on visual observations, for over a period of 18 months at the time of writing this manuscript.

Physical and chemical characterizations

TEM images of the individual nanocellulosic materials (SCNCs, SCNFs and TOCNFs) were obtained using a FEI TALOS F200X FEG system, with an acceleration voltage of 200 kV. Aqueous nanocellulose suspensions, diluted to 0.05 wt% were first drop cast on copper TEM grids, and the excess liquid was blotted away with filter paper. Following this, a drop of 1 wt% ammonium molybdate was applied to improve the contrast, the excess was blotted away with filter paper, and samples were air dried before imaging.

TEM tomography samples of the nanocellulose/MWCNT hybrid materials were prepared on a 200-mesh-Au grid with a carbon supporting film having different sized holes (C-flat: CF-MH-2Au, Electron Microscopy Sciences). Detailed sample preparation protocol is given in the ESI. A region of interest (ROI) with a uniform planar layer of sample covering a suitable hole in the grid was selected for each sample and the samples were imaged using a JEM-2800 electron microscope (JEOL). Tilt-series were automatically collected at 200 kV TEM mode using a RECORDER application (TEMography) with settings: Goniometer tilts spanning − 72 to + 72°, increment steps 2°, CCD (GATAN), ORIUS SC200, 2048 × 2048 camera, pixel X,Y scale 1.104715 nm, at a magnification of 100k. A maximum entropy method (MEM) (Engelhardt 2006, 2007) was used for 3D reconstruction of the tilt series images. Detailed data handling protocols for the tomography method are also explained in the ESI

Aqueous suspensions of nanocellulose/MWCNT were fully dried in an oven at 80 °C for 72 h, before being pre-treated at 80 °C under vacuum for 24 h with a pre-treatment station (Prep Vac II Microtrac BEL, Japan). The samples were then investigated by nitrogen adsorption-desorption (physiosorption) isotherms at 77 K using a BELsorp Mini II (Microtrac BEL, Japan) instrument. Results were analyzed by the Brunauer–Emmett–Teller (BET) method to estimate the specific surface area and porosity of the hybrid materials.

XAS analysis was carried out at the Stanford Synchrotron Radiation Lightsource (SSRL) beamline 8-2 equipped with a bending magnet and spherical grating monochromator. The beam incidence angle was set to 55° and 40 × 40 μm^2 slits were used to obtain a resolution of 200 meV. X-ray bean spot size was approximately 1 × 1 mm^2, with a total flux in the order of 1010 photons/s (Sainio et al. 2021; Leppänen et al. 2021). X-ray energies at the carbon and oxygen 1s edges were measured from 260 to 340 eV and 520 to 560 eV, respectively. Details on XAS samples preparation are given in the ESI.

Electrode preparation and electrochemical measurements

The nanocellulose/MWCNT hybrid electrodes were prepared on tetrahedral amorphous carbon (ta-C) thin film substrates produced by pulsed filtered cathodic vacuum arc (p-FCVA) deposition of 7 nm ta-C layer on top of a p-type silicon wafer coated with an ~ 20 nm Ti adhesion layer (Laurila et al. 2014; Protopopova et al. 2015). Wide operation potential and high chemical inertness, combined with the advantages of low-cost, room-temperature deposition process, make ta-C an attractive substrate for various nanomaterial modifications in electrochemical sensing applications (Peltola et al. 2017; Wester et al. 2017; Laurila et al. 2017; Durairaj et al. 2019). Circular exposed area (3 mm diameter) of ta-C substrates (defined by PTFE tape) were first functionalized with a polyethyleneimine (PEI) layer freely adsorbed from 15 µl drop of 0.1 wt% solution for 10 min and subsequently rinsed with milliQ water and dried in gentle nitrogen flow. Following this, 7 µl drops of aqueous nanocellulose/MWCNT suspensions were drop-cast on the PEI-modified ta-C substrates, and dried for 1 h in an oven at 80 °C, under ambient pressure, and stored in

a shelf at room temperature prior to electrochemical measurements (Durairaj et al. 2021). A Gamry Reference 600 potentiostat was used to carry out the electrochemical CV measurements. A conventional 3-electrode setup was used in all measurements, with a platinum counter wire and a Ag/AgCl reference electrode (+ 0.199 V vs. standard hydrogen electrode (SHE), Radiometer Analytical). The analytes DA—dopamine hydrochloride, PA—paracetamol (acetaminophen) and UA–uric acid were purchased from Sigma-Aldrich. The concentrations of these probes were chosen to be 100 µM for DA and PA, and 500 µM for UA, keeping within physiologically relevant concentrations. The measurements were carried out in 10 mM phosphate buffer saline (PBS) solution (pH = 7.4) at room temperature. A standard background cycling protocol was used with all measured electrodes, wherein the electrodes were first cycled in blank PBS solution in the potential window – 0.2 to + 1 V, for 25 cycles at a scan rate of 500 mV/s, to ensure successful electrode fabrication and establish a stable background current. All electrodes were immersed in PBS solution 45 min prior to measurements and were kept immersed for the entire duration of electrochemical measurements.

Results and discussions

Physical and chemical characteristics

TEM images of the different nanocellulosic materials SCNCs, SCNFs and TOCNFs, are shown in Fig. 1a–c, respectively. The SCNCs (Fig. 1a) can be seen as rigid rod like structures with dimensions in the range of 5.1 ± 1.7 nm width and 100–120 nm length. The SCNFs and TOCNFs (Fig. 1b, c) appear as thin and long thread-like structures, with widths of 4.2 ± 1.1 nm, and 2.9 ± 0.8 nm, respectively, and lengths in the range of several microns (SCNFs containing also sub-micron fractions). Planar TEM images of the three nanocellulose/MWCNT hybrid materials, taken when the samples were perpendicular to electron beam during the tilt series, are shown in Fig. 1d–f, respectively, and the corresponding three-dimensional tomographic reconstructions are presented in Fig. 1g–i, respectively. Videos for the animated tilt series and corresponding three-dimensional reconstructions can be found in the ESI provided with this publication.

The red arrows in Fig. 1d-i point out some of the MWCNTs clearly distinguishable as long and well-defined continuous tube like structures in the hybrid materials. Dimensions of the MWCNTs, as specified by the manufacturer, are in the range of 30 ± 15 nm width and 5–20 µm length, and are in agreement with the observed structures. Individual nanocellulosic materials cannot be clearly distinguished in the hybrid material TEM images due to aggregation expected from the use of acetic acid and methanol in tomography sample preparation process. The SCNC/MWCNT hybrid architecture (Fig. 1d and g) appears as a dense mat of cellulose nanocrystals packed closely around the MWCNTs, making it difficult to identify individual MWCNTs unambiguously. In contrast, both the SCNF/MWCNT (Fig. 1e and h) and TOCNF/MWCNT (Fig. 1f and i) hybrid materials appear to form more open architectures, where individual MWCNTs can be clearly recognized, surrounded by a matrix of thinner cellulose nanofibrils and bundles. X-ray computed tomography (CT) studies in the micron scale have previously been reported for nanocellulosic materials (Osorio et al. 2018) and some TEM-tomographic studies for individual MWCNT (Rossell et al. 2013; Kwon and Zewail 2010) and composites with metal particles (Ersen et al. 2007; Tessonnier et al. 2009) have also been previously reported. However, no previous attempts have been reported regarding the TEM based tomographic investigations of nanocellulosic materials, and in particular nanocellulose/MWCNT hybrid materials. The three-dimensional tomographic reconstructions presented here enable the direct visualization of different network architectures resulting from the dispersion of MWCNTs by different nanocellulosic materials.

The specific surface area (S_{BET}), total pore volume (V_T) (at a relative pressure of $P/P_0 = 0.990$) and mean pore diameter for all three hybrid materials were obtained from the N_2 physiosorption isotherms (see ESI Fig. S1). All hybrid materials exhibit Type IVa isotherms indicating predominantly meso/macroporous architectures (Kondor et al. 2021) The SCNC/MWCNT hybrid has the highest specific surface area of 112 m^2/g, and pore volume of ~ 0.85 cm^3/g, compared to the SCNF/MWCNT hybrid with a specific surface area of 55 m^2/g, and pore volume of ~ 0.5 cm^3/g, and TOCNF/MWCNT hybrid with a

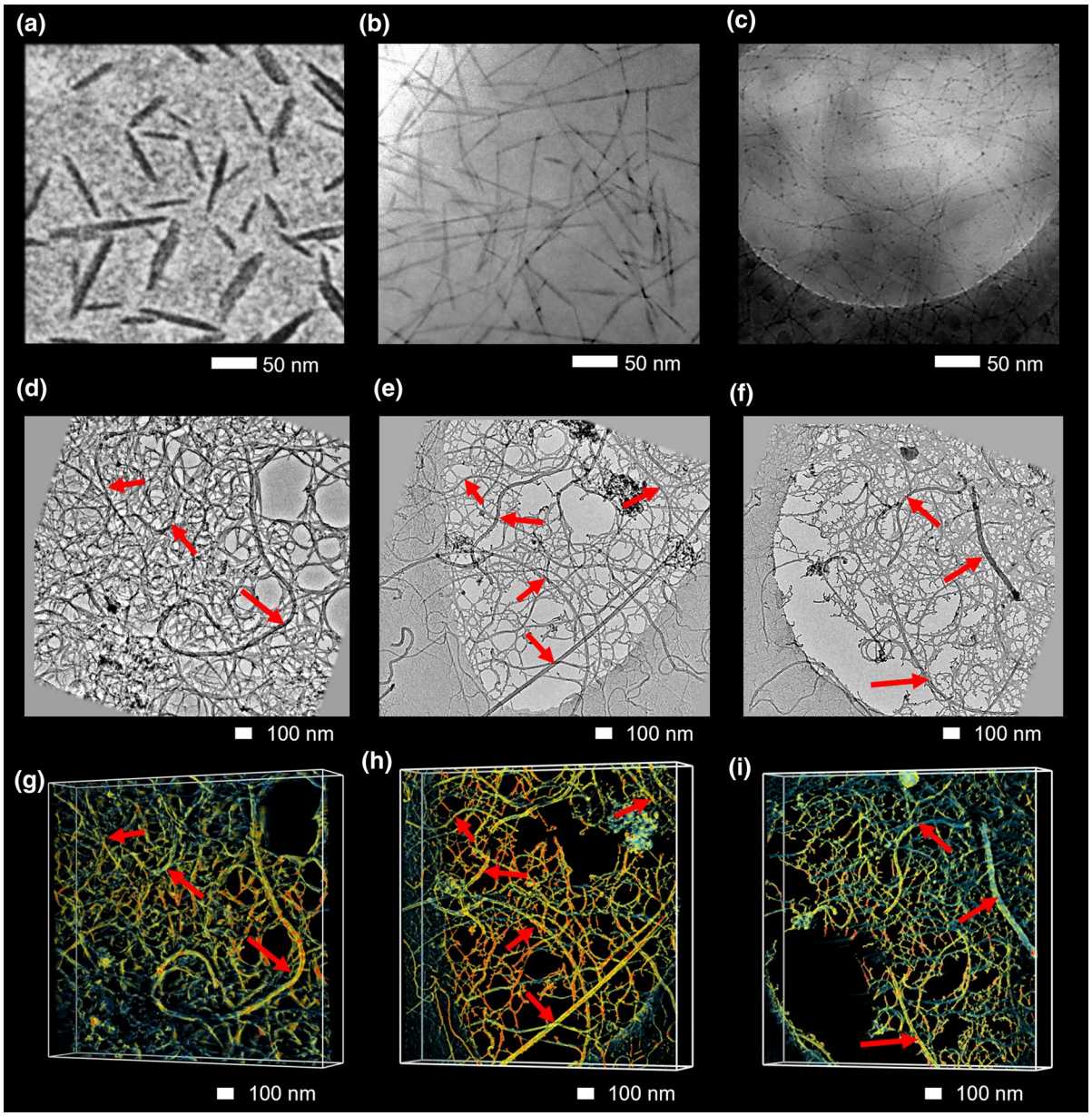

Fig. 1 TEM images of **a** SCNCs, **b** SCNFs, and **c** TOCNFs, respectively, showing individual nanocellulosic components. Planar TEM images (**d–f**) and three dimensional TEM tomographs (**g–i**) of the hybrid materials (SCNC/MWCNT, SCNF/MWCNT, TOCNF/MWCNT, respectively), showing the dispersion of MWCNTs in different nanocellulosic matrices. Red arrows in figures d to i indicate MWCNTs

specific surface area of 3 m^2/g, and pore volume of ~ 0.025 cm^3/g. The oven drying protocol was chosen here so as to mimic the conditions used in the electrode making. During the drying process, the CNF-based hybrid materials resulted in large flaky solids, whereas the CNC-based hybrid dried as a more powdery substance (photographs in ESI Fig. S1). The observed low specific surface area and pore volumes for the CNF-based hybrid materials could be a result of the denser dried structures. The mean pore diameters were estimated to be 30 nm, 37 nm and 35 nm for the SCNC, SCNF and TOCNF -based hybrid

materials, respectively, in agreement with the TEM tomography observations, where the CNF-based hybrid materials have more open architectures. However, it must be noted that the BET values are only indicative and the actual hybrid material porosity in the end application environment (PBS in this study) is likely very different due to the different relative swelling of the nanocellulosic materials (Kondor et al. 2021).

The XAS studies in this work are focused mainly on understanding how the individual nanocellulose building blocks may or may not affect the surface chemistry of the electrochemically active component (herein MWCNTs) in the different hybrid materials. As the electrocatalytic properties of MWCNTs are known to strongly depend on surface oxygen-based functionalities (Laurila et al. 2017), we focus here on the carbon and oxygen spectra to identify any changes in the surface chemistry of the MWCNTs resulting from the presence of different functionalized nanocellulosic components. The normalized total electron yield (TEY) spectra measured at C 1*s* and O 1*s* edges are shown in Fig. 2a and b, respectively, and the dominant peak associations listed in Fig. 2c. The reference MWCNT sample shows a strong sp^2 π^* at 285.2 eV, which is also dominant in the hybrids with different nanocellulosic materials. Although the profiles of the nanocellulose spectra seem to slightly differ from each other, the locations of the main peaks are similar for the different grades. The low intensity shoulder observed in the reference nanocellulose materials spectra around 285 eV can be attributed to C–H bonds in the cellulose structure (Karunakaran et al. 2015). The two other dominant peaks observed in all nanocellulose (and hybrid material) spectra at 289.3 eV and 290.7 eV can be attributed to the 1s → π^* transitions of C–OH and C–H bonds in the cellulose structure, respectively (Karunakaran et al. 2015).

The long range order sp^2 peak at 291.6 eV, and the broad feature centered around ~ 292.8 eV attributed to the σ^* transitions in the sp^2 (CNTs) (Sainio et al. 2021) are also clearly distinguishable in the reference MWCNTs and all hybrid materials, despite the background from the carbon spectra of the cellulosic materials. No clear features were observable in the O 1*s* spectrum of the reference MWCNTs sample, and all other samples showed a similar spectral pattern with two low intensity peaks at around 531.5 and 532 eV, corresponding to the 1s → π^* transition peaks of C=O and a broader high intensity peak at 538 eV corresponding to the σ^* resonances in the cellulose structure (Karunakaran et al. 2015). The similarity of strong sp^2 carbon related peaks observed in the C 1*s* spectra of all hybrid materials compared to the reference MWCNTs, as well as the lack of new spectral features or shifts in both C 1*s* and O 1*s* spectra, are clear indications that the surface chemical nature of MWCNTs remains unaltered in the hybrids with the different nanocellulosic materials.

Electrochemical behavior

Cyclic voltammograms measured with the different studied hybrid electrodes, at a scan rate of 100 mV/s, in 10 mM PBS solutions containing 100 µM dopamine, 100 µM paracetamol and 500 µM uric acid, are shown in Fig. 3a–c, respectively. Clear differences can be observed in the responses of the different electrodes towards each of the analytes. The cellulose nanocrystal-based hybrid (SCNC/MWCNT) shows a noticeably lower response towards each of the measured analyte compared to both the cellulose nanofibril-based hybrids. Evolution of pre-peaks indicating oxidation product adsorption are observed in the CVs of dopamine and uric acid at the SCNF/MWCNT hybrid electrode, and to a lesser extent at TOCNF/MWCNT hybrid electrode, but are not distinguishable at the SCNC/MWCNT hybrid electrode. The baselines for the peaks observed in the CVs are approximated by the tangent to the flat region preceding the peaks, and the peak anodic (I_{pa}) and cathodic (I_{pc}) currents are calculated as the maximum current of the main peak corrected for the corresponding baseline. The anodic and cathodic peak potentials (E_{pa} and E_{pc}, respectively) denote the potentials at which the maximum current of the main peaks are observed, and delta E_p is calculated as $(E_{pa} + E_{pc})/2$. The values of these parameters for each analyte, at the three different electrodes, are tabulated in Table. S1, along with the onset potentials of the main peaks. The onset potentials were estimated as the intersection of the tangent to the fast-rising slope of the main peak to the baseline, and are found to be similar at all hybrid electrodes for the different analytes. This is consistent with the chemical analyzes indicating that the electrochemically active species, herein MWCNTs, has similar surface chemistry in all hybrids.

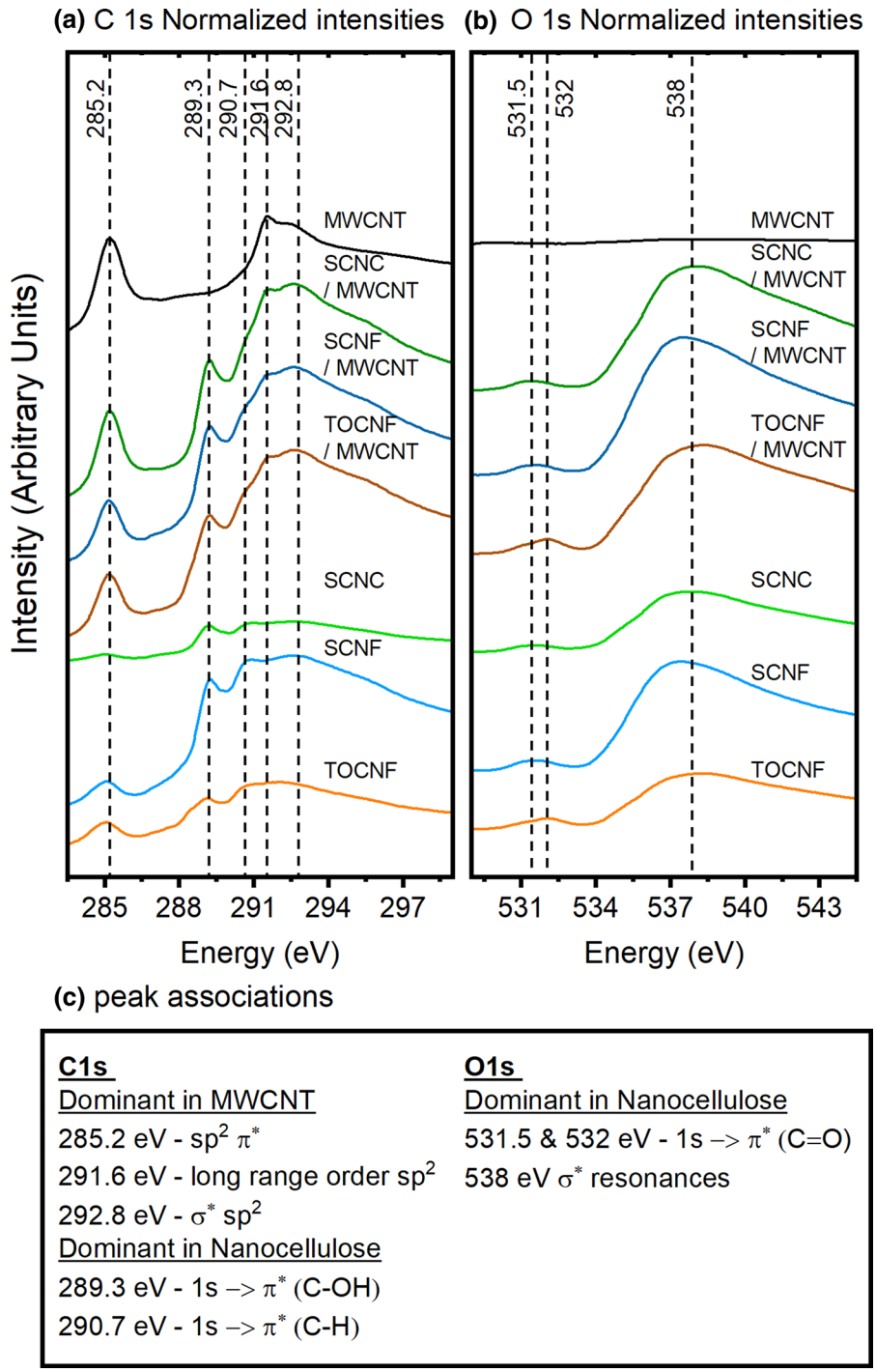

Fig. 2 C 1*s* (**a**) and O 1*s* (**b**) normalized XAS spectra for different nanocellulosic materials and their hybrids with MWCNTs, along with reference MWCNTs and the dominant peak associations are shown in (**c**)

Electroanalytical performances of the different hybrid electrodes were further analyzed at different scan rates from 10 to 500 mV/s, for each of the analyte, and the CVs are shown in ESI (Fig. S2). Anodic and cathodic peak currents were estimated for different scan rates and the equations for linear fits of log of peak currents (I_{pa} and I_{pc}) versus log of scan rate (ν) are also presented in ESI Table S1. The slopes of these linear fits provide useful insight into the electrochemical processes occurring at the electrodes,

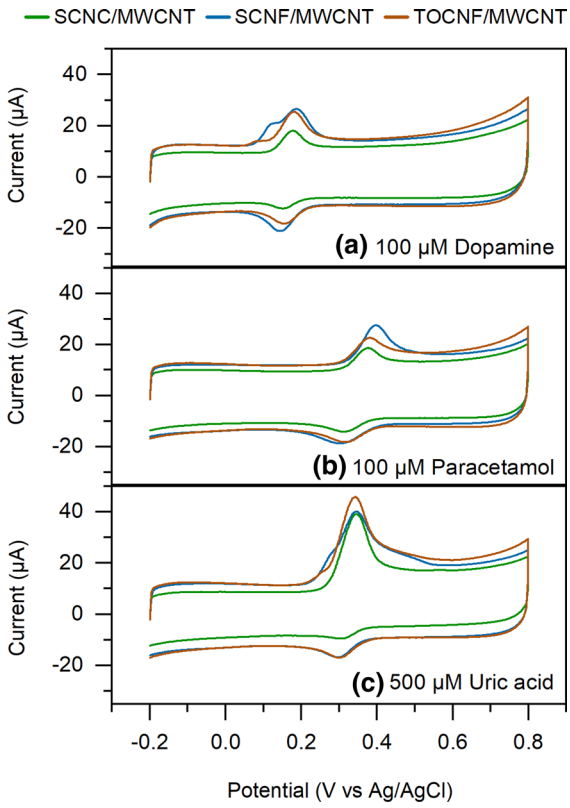

Fig. 3 Comparison of cyclic voltammograms for the hybrid electrodes SCNC/MWCNT, SCNF/MWCNT, and TOCNF/MWCNT, measured at 100 mV/s scan rate, in 10 mM PBS at pH 7.4, containing **a** 100 μM Dopamine, **b** 100 μM Paracetamol, and **c** 500 μM Uric acid, respectively

wherein a theoretical slope of 0.5 indicates a diffusion (linear semi-infinite) controlled process and a slope closer to 1 indicates the involvement of adsorption processes (or thin film electrochemical behavior) (Gosser 1993). In the case of paracetamol, all studied hybrid materials show a slope of 0.6, indicating mainly diffusion controlled process. Whereas for both dopamine and uric acid the slopes are closer to unity indicating more adsorption related processes. In order to further distinguish between adsorption and thin liquid layer formation effects, enrichment and washout studies were carried out for each analyte at the different hybrid electrodes, and the results are shown in Fig. 4. The enrichment protocol was carried out as follows: CVs were measured immediately upon the insertion of a pristine electrode into the electrochemical cell containing the analyte (labelled 'immediate scan' in Fig. 4), following which the electrode was allowed to stay at open circuit potential (OCP) in the electrochemical cell containing the analyte for 5 min, and then a second CV was measured (labelled '5 min enriched' in Fig. 4). After the enrichment scan, the electrode was taken out of the electrochemical cell and rinsed in a beaker containing blank PBS solution for 10 min with intermittent agitation. Following the 10 min wash, the electrode performance was again measured with CV in a blank PBS containing electrochemical cell (labelled as 'Residual in blank PBS after 10 min wash' in Fig. 4). The baseline subtracted main oxidation peak currents for all analytes, in the immediate, enriched and residual scans are presented in Table 1.

For all analytes studied, the SCNF/MWCNT hybrid shows the highest enriched and residual oxidation currents, whereas the SCNC/MWCNT hybrid shows the least. For the same concentration (100 μM) of dopamine and paracetamol, all hybrids exhibit higher enrichment in oxidation currents for the cationic dopamine, compared to neutral paracetamol. Further, for a 5 times larger concentration of uric acid (500 μM), the SCNF/MWCNT and TOCNF/MWCNT hybrids exhibit only ~ 1.3 times and ~ 1.7 times higher enriched currents, respectively, compared to that of 100 μM dopamine, indicating higher electroanalytical response to the cationic molecule. However, the SCNC/MWCNT hybrid exhibits a ~ 3 times higher enriched current for uric acid when compared to dopamine, indicating lesser enrichment of the cationic analyte. In our previous work (Durairaj et al. 2021), we observed that the cationic OSR probe ($Ru(NH_3)_6^{2+/3+}$) exhibits over ~ 2 and 3 times higher currents at the SCNF/MWCNT hybrid in PBS, compared to TOCNF/MWCNT and SCNC/MWCNT hybrids, respectively. A similar trend is observed here, but to a lesser extent, in the behavior of the cationic ISR analyte (dopamine), where the SCNF/MWCNT hybrid exhibits ~ 1.5 and 2 times higher enriched current compared to TOCNF/MWCNT and SCNC/MWCNT hybrids, respectively. The neutral paracetamol also exhibits the highest enriched current at SCNF/MWCNT, ~ 1.2 and ~ 2.5 times higher than at TOCNF/MWCNT and SCNC/MWCNT hybrids, respectively. The anionic uric acid however, behaves very similarly at both the CNF-based hybrids, and has only slightly lesser currents at the SCNC/MWCNT hybrid, indicating a relatively low

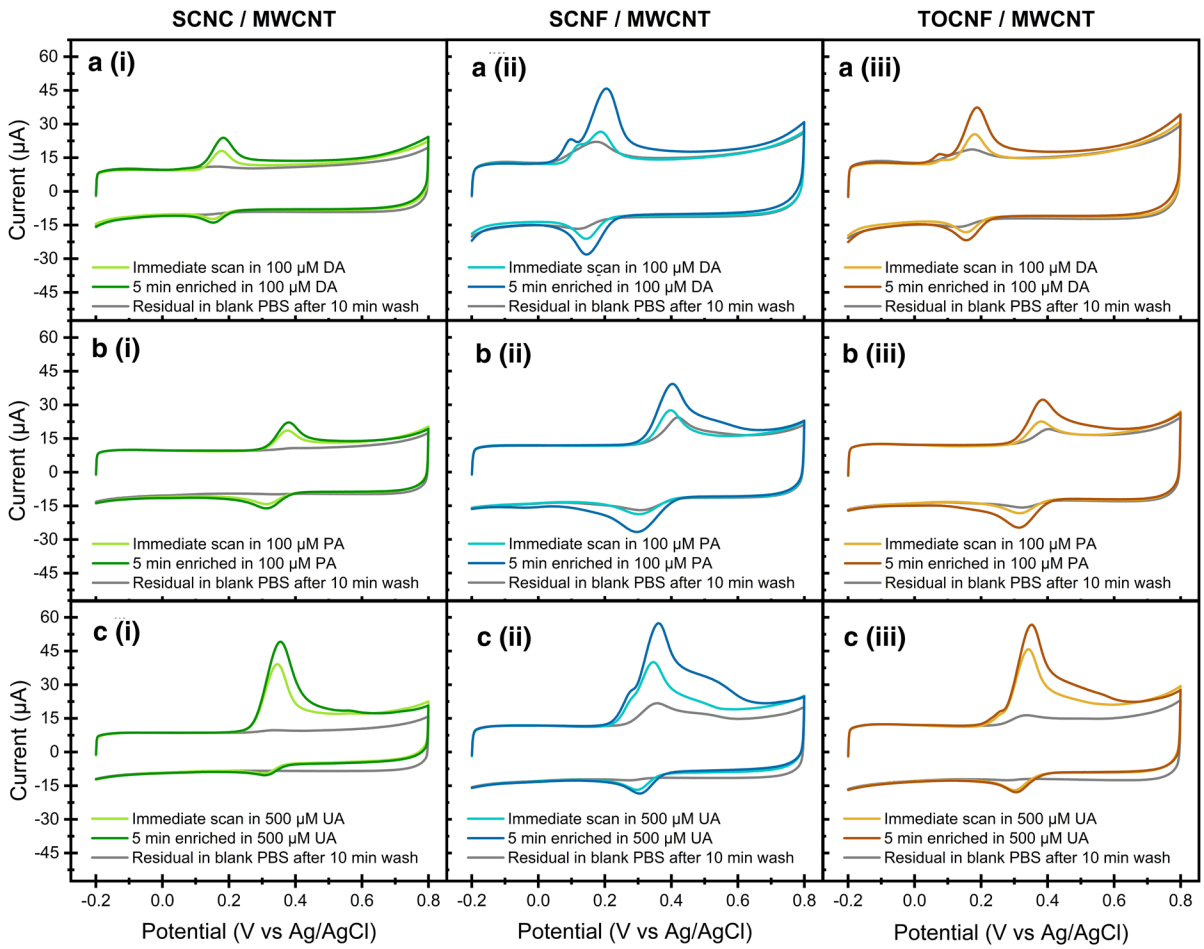

Fig. 4 Cyclic voltammograms at 100 mV/s, showing the immediate scan and 5 min enrichment measured in 10 mM PBS at pH 7.4 containing **a** 100 μM Dopamine (DA), **b** 100 μM Paracetamol (PA), and **c** 500 μM Uric acid (UA), for the hybrid electrodes (**i**) SCNC/MWCNT, **ii** SCNF/MWCNT, and **iii** TOCNF/MWCNT, respectively. Gray plot in each figure shows the CV measured in blank PBS after 10 min of washout (in PBS) for the corresponding electrodes used in each of the enrichment studies, respectively

Table 1 Baseline subtracted peak current values of the main oxidation peak for dopamine, paracetamol and uric acid, in the immediate (Imm), 5 min enrichment (Enr) and post-washing residual (Res) scans, estimated from Fig. 4

Analyte	SCNC/MWCNT			SCNF/MWCNT			TOCNF/MWCNT		
	Imm (μA)	Enr (μA)	Res (μA)	Imm (μA)	Enr (μA)	Res (μA)	Imm (μA)	Enr (μA)	Res (μA)
DA	9	14.5	1.7	14.2	33.7	9.8	13.1	24.9	6.2
PA	8.8	13.1	1.6	16.3	27.7	12.7	10.9	21.4	7.9
UA	30.9	41.2	1.4	29.1	46.2	10.9	34.1	45.7	5.4

DA-100 μM Dopamine, PA 100-μM Paracetamol, UA-500 μM Uric acid

enrichment compared to dopamine and paracetamol at all hybrids. As indicated by the XAS results and the onset potentials of electrochemical reactions of various analytes, the MWCNTs appear to be chemically identical in all hybrids. The observed differences in the electroanalytical response and

enrichment behavior of the various analytes at the different hybrid electrodes can thus be primarily attributed to the role of nanocellulose in the hybrids.

The TEM tomography technique presented in this study provides a qualitative visual method to investigate the distribution of different nanomaterials in the hybrids. It can be clearly observed in the TEM tomographs that the short and rigid CNCs are packed more closely around the long MWCNTs (Fig. 1d, g), partially covering the MWCNT surfaces, which is expected to reduce the electrochemically active surface area for the target molecules. In comparison the longer and flexible CNFs form more open hybrid architectures with MWCNTs (Fig. 1e, f, h, i). Further the BET measurements indicate that the SCNC/MWCNT hybrid has a smaller mean pore diameter compared to both the CNF-based hybrids, even in the dried state. In conjunction with the known phenomenon of the lesser swelling of CNC-based films compared to that of CNF-based films (Hakalahti et al. 2017; Niinivaara et al. 2015), this supports the hypothesis of lower accessibility of MWCNT surfaces for the different analytes in the CNC-based hybrid, which will contribute to the observed smaller peak currents compared to CNF-based hybrids. To further verify this hypothesis, the electrochemically active surface area (ECSA) of all hybrids are estimated from CV measurements, using the Randles–Sevcik (R-S) equations (García-Miranda Ferrari et al. 2018). Typically, an ideal OSR probe such as $Ru(NH_3)_6^{2+/3+}$ is used to estimate the ECSA using the reversible R–S equation (Eq. 1),

$$I_{p,f}^{\text{rev}} = \pm 0.446 nFA_{\text{real}} C \sqrt{\frac{nFD\nu}{RT}} \quad (1)$$

where $I_{p,f}^{\text{rev}}$ is the peak forward (oxidation) current of the reversible voltammetric reaction, n is the number of electrons transferred in the reaction ($n = 1$ for $Ru(NH_3)_6^{2+/3+}$), F is the Faradays constant (C/mol), C is the concentration of the analyte in mol/cm^3, ν is the applied scan rate (V/s), R is the universal gas constant, D is diffusion coefficient (cm^2/s) and A_{real} is the real electrochemically active surface area in cm^2. A modified R–S equation (Eq. 2) can be applied for irreversible reactions of inner sphere redox probes such as dopamine, to obtain qualitative information for comparing different materials:

$$I_{p,f}^{\text{irrev}} = \pm 0.496 \sqrt{\alpha n'} nFA_{\text{real}} C \sqrt{\frac{nFD\nu}{RT}} \quad (2)$$

where α is the transfer coefficient (usually approximated to 0.5), n' is the number of electrons transferred before rate determining step ($n' = 1$ and $n = 2$ for dopamine, assuming that the second electron transfer is the rate determining step) and the remaining parameters are same as Eq. (1). Table 2 lists the ECSA values estimated from the main oxidation peak currents of 100 mV/s CV measurements with 1 mM $Ru(NH_3)_6^{2+/3+}$ (Fig. 5(b) in our previously published work Durairaj et al. 2021) and 100 µM dopamine (Fig. 3 above) in PBS at 25 °C, using the literature values of diffusion coefficients 9.1×10^{-6} cm^2/s and 6.74×10^{-6} cm^2/s, for ruthenium and dopamine, respectively. It must be noted that the ECSA values obtained here are only qualitative, especially for the ISR probe dopamine, as application of Randles–Sevcik equation is unreliable in these cases. The numbers in Table 2 are therefore not absolute, and can only be used as indicative values for comparing different materials. In agreement with our hypothesis, the SCNC/MWCNT hybrid shows the lowest ECSA for both OSR and ISR probes, whereas the SCNF/MWCNT hybrid shows the highest ECSA.

Together with the TEM tomographs, these results clearly indicate that the nanocellulose geometry and degree of functionalization strongly dictate the network morphology of the nanocellulose/MWCNT hybrids, thereby tailoring the electrochemical surface area and electroanalytical response of both inner and outer sphere redox probes. Furthermore, the observed differences between SCNF/MWCNT versus TOCNF/MWCNT hybrids indicate that the type of functional group also affects electrochemical behavior of the hybrid, wherein the presence of SCNFs (1.7 mmol/g OSO_3^-) shows higher sensitivity and stronger enrichment for the cationic dopamine, compared to that of TOCNFs (1.3 mmol/g COO^-), due to the stronger

Table 2 Electrochemically active surface areas (cm^2) estimated using Randles–Sevcik equations

	SCNC/MWCNT	SCNF/MWCNT	TOCNF/MWCNT
Ruthenium	0.09	0.42	0.19
Dopamine	0.21	0.34	0.27

electrostatic effects of the more negative sulfate groups. This effect is also observed to be more significant in electrolytes of lower ionic strength (PBS vs. 1 M KCl), as demonstrated in our previous work (Durairaj et al. 2021).

In order to understand the cumulative contributions of the observed morphological and electrostatic effects upon the overall hybrid electrode selectivity and sensitivity, a concentration series measurement was performed. Varying concentrations of dopamine (100 nM to 100 µM) were measured using CV at 100 mV/s scan rate, by successive additions to an interferent solution containing 1 mM ascorbic acid and 500 µM uric acid in PBS. For comparison, commercially available MWCNT-modified screen-printed electrodes (DRP110CNT from Metrohm DropSens) with carboxylated MWCNTs were also measured under similar conditions. The commercial electrodes were masked using teflon tape, such that only the working electrode area (3 mm diameter, circular) was exposed, and the same external reference (Ag/AgCl) and counter (Pt) electrodes as in all other measurements were used. The results from the concentration series are shown in Fig. 5. In the commercial

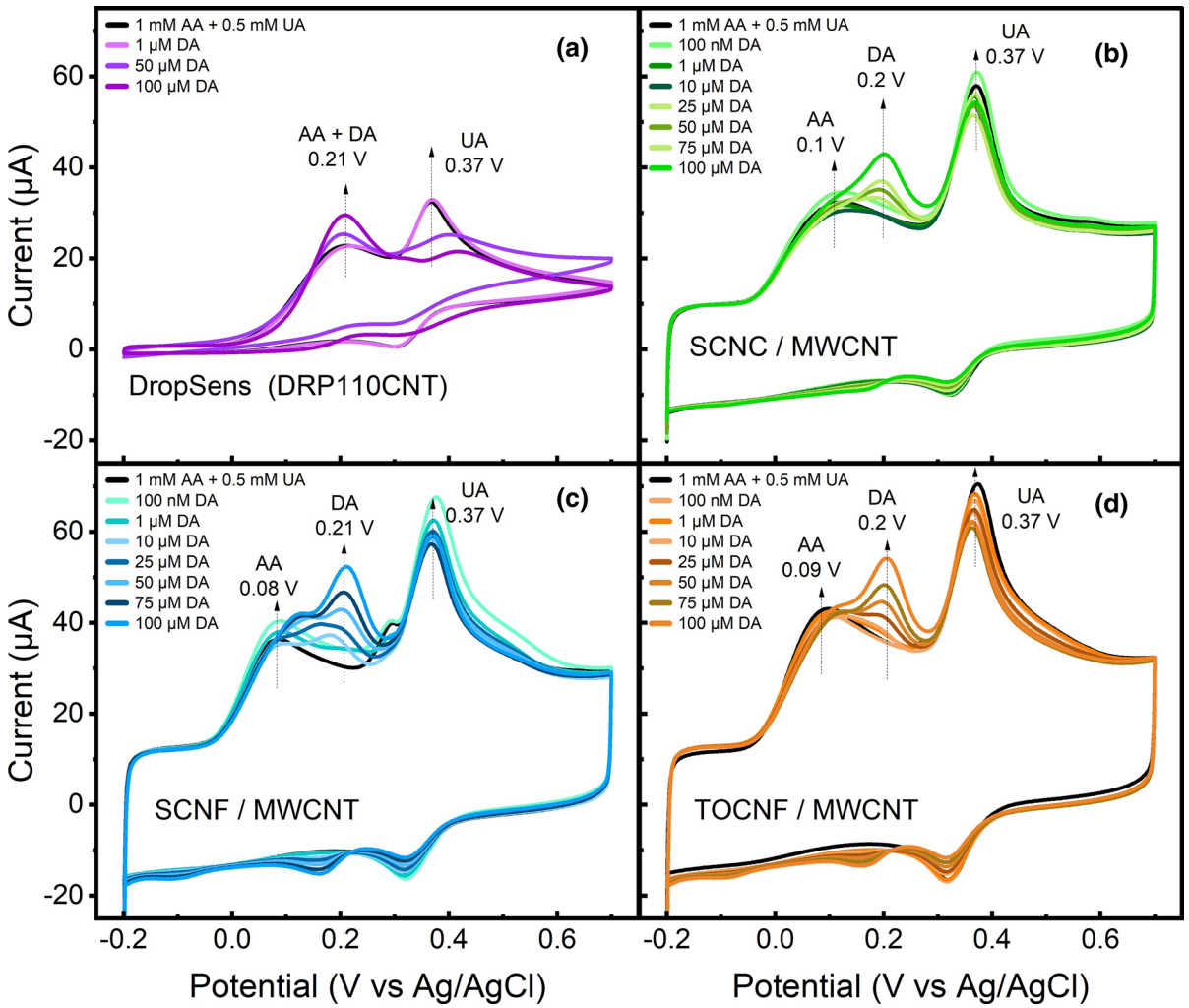

Fig. 5 Cyclic voltammograms at 100 mV/s scan rate, showing the dopamine (DA) concentration series measurements made in the interferent solution containing 1 mM ascorbic acid (AA) and 0.5 mM uric acid (UA) in PBS, for the commercial DRP110CNT electrode (**a**), and the hybrid electrodes SCNC/MWCNT (**b**), SCNF/MWCNT (**c**), and TOCNF/MWCNT (**d**), respectively

DRP110CNT electrode, it is clearly evident that the large interference from ascorbic acid oxidation, occurring at around 0.21 V, makes it impossible to selectively detect dopamine, which oxidizes at the same potential at these electrodes. In contrast, the oxidation peak for ascorbic acid is considerably cathodically (negative) shifted at all the studied nanocellulose/MWCNT hybrid electrodes, to around 0.1 V. This cathodic shift is often attributed to the electrocatalytic effect of carbon nanomaterials, due to the presence of large edge-plane graphitic sites, defects and catalyst metal impurities (Banks and Compton 2005, 2006; Dumitrescu et al. 2009; Tsierkezos et al. 2016). In their work on MWCNTs grown directly on ta-C substrates, Palomäki et al. (2018) observed a similar shift in the ascorbic acid oxidation potential. In this study, the cathodic shift of ascorbic acid oxidation, along with the electrostatic effects from the predominantly negatively functionalized nanocellulosic materials in the hybrids, enable the selective and sensitive detection of physiologically relevant concentrations of the cationic dopamine molecules, in challenging interferent solutions and even in relatively fast CV measurements. Limits of detection (LOD) of dopamine at the different hybrid electrodes were estimated in the linear range of 0.1–100 µM dopamine concentrations using the equation $\mathrm{LOD} = 3.3 * \sigma/S$, where σ denotes the standard deviation ($n = 3$) of anodic current at the dopamine oxidation potential (0.21 V) measured in the interferent solution before dopamine additions, and S denotes the slope of the linear fit of peak current (dopamine primary oxidation at 0.21 V) versus concentration data (µA/µM) for each hybrid electrode. The CNF-based hybrid electrodes (SCNF and TOCNF) both exhibit a LOD of 176 nM, whereas the SCNC/MWCNT hybrid electrode exhibits a higher LOD of 250 nM. Although slight differences were observed in the SCNF versus TOCNF -hybrid electrodes towards individual analytes as discussed earlier, the LOD measured for dopamine in the interferent solution was the same for both these hybrid electrodes, with similar geometry and degree of functionalization, but different functional groups. These results further indicate that the hybrid electrode morphology, dictated by nanocellulose geometry and degree of functionalization, has the most significant effect on the overall sensitivity and selectivity of the nanocellulose/MWCNT hybrid electrodes towards inner sphere redox molecules.

The development of nanocellulose/carbon nanomaterial platforms for electroanalytical applications is still a relatively new field, and the versatility of nanocellulosic materials used in such platforms alone can add several interesting functionalities, as demonstrated in our current and previous work (Durairaj et al. 2021), and by Dortez et al. (2022). Therefore, thorough characterizations with a wide variety of nanocellulose and carbon nanomaterial components, as well as redox probes, are vital to the further development of such hybrid platforms. The characterization methods and electrochemical investigations carried out in this work, together with our previous work (Durairaj et al. 2021), are intended to provide a comprehensive, although by no means complete, overview of the role nanocellulosic materials in tailoring the electroanalytical performance of nanocellulose/carbon nanomaterial hybrids. We clearly demonstrate that the functionalization and geometry of the nanocellulosic material must be carefully chosen, keeping in mind the dimensions and charge of the analyte to be detected, in order to attain optimal sensitivity and selectivity.

Conclusions

The emergence of nanocellulosic materials as effective dispersants for carbon nanomaterials is a highly promising route for the development of industrially scalable and environmentally friendly electroanalytical platforms. The versatility of nanocellulosic materials available already for research, and their increasingly promising demonstrations in electroanalytical platforms with carbon nanomaterials, mandate the need to understand their role in tailoring the electrochemical response of such hybrids. In this work, the hybrid architectures are examined with a novel TEM tomography technique, revealing directly that the rigid cellulose nanocrystals form dense architectures with close packing around MWCNTs, thereby limiting the available MWCNT surfaces. In contrast the long and flexible cellulose nanofibrils are seen to form open architectures with more exposed MWCNT surfaces, and correspondingly higher electrochemically active surface area and stronger electroanalytical responses are observed for all studied analytes at the CNF-based hybrids when compared to CNC-based hybrid.

Further, the XAS studies verify that the surface carbon and oxygen-based functionalities of the MWCNTs are unmodified by the dispersion in different functionalized nanocellulosic materials. Therefore, the observed differences in the electrochemical behaviors of various probe molecules can be attributed primarily to the variations in the geometry and functionalization of the nanocellulosic components, which play a vital role in determining the morphology and electrostatic effects of the hybrid. These results, along with our previous study (Durairaj et al. 2021), demonstrate that (1) a variety of nanocellulosic materials with different geometries and functionalizations can be used to develop highly stable and robust electroanalytical platforms with carbon nanomaterials, (2) the chemical and physical nature of the carbon nanomaterial is essentially unmodified by the presence of different nanocellulosic materials, thereby preserving its inherent electrochemical activity, (3) the choice of nanocellulosic material (geometry and functionalization) can significantly affect the electroanalytical performance of such hybrids towards various physiologically relevant small molecules.

Supplementary information

Sample preparation and data handling details for TEM and XAS. BET data. Cyclic voltammograms at different scan rates for all analytes at different hybrid electrodes. Electrode-to-electrode repeatability measurements. Tabulated cyclic voltammetry parameters for all analytes.

Acknowledgments The authors acknowledge the provision of facilities by Aalto University Bioeconomy and OtaNano—Nanomicroscopy Center (Aalto-NMC) and RawMatters research infrastructure (RAMI). D.Sc. Yanling Ge is acknowledged for assistance with TEM of nanocellulosic materials. Use of the Stanford Synchrotron Radiation Lightsource, SLAC National Accelerator Laboratory, is supported by the U.S. Department of Energy, Office of Science, Office of Basic Energy Sciences under Contract No. DE-AC02-76SF00515.

Author contributions Study concept and design was carried out by VD under the guidance of KSK, TT, TL and JKTL and NW, assisted VD in electrochemical measurements, data analysis and discussions. PE performed TEM tomography measurements, SS carried out XAS measurements, BPW performed BET measurements. PL produced the SCNF, SCNC and TOCNF materials and obtained their TEM images. All authors participated in manuscript editing and have read and approved the final manuscript.

Funding Open Access funding provided by Aalto University. This study was funded by the Academy of Finland′s Flagship Programme under Projects Nos. 318890 and 318891 (Competence Center for Materials Bioeconomy, FinnCERES). Author SS, was additionally funded by Walter Ahlström Foundation and European Union's Horizon 2020 research and innovation programme under the Marie Sklodowska-Curie Grant Agreement No 841621.

Declarations

Ethics approval and consent to participate Not applicable.

Consent for publication Not applicable.

Availability of data and materials Not applicable.

Code availability Not applicable.

Conflict of interest The authors declare no competing interests.

References

Abdul Khalil H, Davoudpour Y, Islam MN et al (2014) Production and modification of nanofibrillated cellulose using various mechanical processes: a review. Carbohydr Polym 99:649–665. https://doi.org/10.1016/j.carbpol.2013.08.069

Abu-Danso E, Srivastava V, Sillanpää M et al (2017) Pretreatment assisted synthesis and characterization of cellulose nanocrystals and cellulose nanofibers from absorbent cotton. Int J Biol Macromol 102:248–257. https://doi.org/10.1016/j.ijbiomac.2017.03.172

Banks CE, Compton RG (2005) Exploring the electrocatalytic sites of carbon nanotubes for NADH detection: an edge plane pyrolytic graphite electrode study. Analyst 130(9):1232. https://doi.org/10.1039/b508702c

Banks CE, Compton RG (2006) New electrodes for old: from carbon nanotubes to edge plane pyrolytic graphite. Analyst 131(1):15–21. https://doi.org/10.1039/B512688F

Chang X, Henderson WM, Bouchard DC (2015) Multiwalled carbon nanotube dispersion methods affect their aggregation, deposition, and biomarker response. Environ Sci Technol 49(11):6645–6653. https://doi.org/10.1021/acs.est.5b00654

Desmaisons J, Boutonnet E, Rueff M et al (2017) A new quality index for benchmarking of different cellulose nanofibrils. Carbohydr Polym 174:318–329. https://doi.org/10.1016/j.carbpol.2017.06.032

Dong XM, Revol JF, Gray DG (1998) Effect of microcrystallite preparation conditions on the formation of colloid crystals of cellulose. Cellulose 5(1):19–32. https://doi.org/10.1023/A:1009260511939

Dortez S, Sierra T, Álvarez-Sánchez MÁ et al (2022) Effect of nanocellulose polymorphism on electrochemical analytical performance in hybrid nanocomposites with non-oxidized single-walled carbon nanotubes. Microchim Acta 189(2):62. https://doi.org/10.1007/s00604-021-05161-w

Dumitrescu I, Unwin PR, Macpherson JV (2009) Electrochemistry at carbon nanotubes: perspective and issues. Chem Commun 7345(45):6886. https://doi.org/10.1039/b909734a

Durairaj V, Wester N, Etula J et al (2019) Multiwalled carbon nanotubes/nanofibrillar cellulose/Nafion composite-modified tetrahedral amorphous carbon electrodes for selective dopamine detection. J Phys Chem C 123(40):24826–24836. https://doi.org/10.1021/acs.jpcc.9b05537

Durairaj V, Li P, Liljeström T et al (2021) Functionalized nanocellulose/multiwalled carbon nanotube composites for electrochemical applications. ACS Appl Nano Mater 4(6):5842–5853. https://doi.org/10.1021/acsanm.1c00774

Engelhardt P (2006) Electron tomography of chromosome structure. Wiley, Chichester. https://doi.org/10.1002/9780470027318

Engelhardt P (2007) Three-dimensional reconstruction of chromosomes using electron tomography. Humana Press, Totowa, pp 365–385. https://doi.org/10.1007/978-1-59745-294-6_18

Ersen O, Werckmann J, Houllé M et al (2007) 3D electron microscopy study of metal particles inside multiwalled carbon nanotubes. Nano Lett 7(7):1898–1907. https://doi.org/10.1021/nl070529v

Eyley S, Thielemans W (2014) Surface modification of cellulose nanocrystals. Nanoscale 6(14):7764–7779. https://doi.org/10.1039/C4NR01756K

Fatin M, Rahim Ruslinda A, Norhafizah S, et al (2014) Oxidation functionalization of multiwalled carbon nanotube by mild acid sonication. In: 2014 IEEE conference biomedicine engineering science. IEEE, pp 686–689. https://doi.org/10.1109/IECBES.2014.7047593

Ferreira FV, Otoni CG, De France KJ et al (2020) Porous nanocellulose gels and foams: breakthrough status in the development of scaffolds for tissue engineering. Mater Today 37(August):126–141. https://doi.org/10.1016/j.mattod.2020.03.003

García-Miranda Ferrari A, Foster C, Kelly P et al (2018) Determination of the electrochemical area of screen-printed electrochemical sensing platforms. Biosensors 8(2):53. https://doi.org/10.3390/bios8020053

Gosser DK (1993) Cyclic voltammetry: simulation and analysis of reaction mechanisms, vol 43. VCH, New York

Habibi Y (2014) Key advances in the chemical modification of nanocelluloses. Chem Soc Rev 43(5):1519–1542. https://doi.org/10.1039/C3CS60204D

Habibi Y, Lucia LA, Rojas OJ (2010) Cellulose nanocrystals: chemistry, self-assembly, and applications. Chem Rev 110(6):3479–3500. https://doi.org/10.1021/cr900339w

Hajian A, Lindström SB, Pettersson T et al (2017) Understanding the dispersive action of nanocellulose for carbon nanomaterials. Nano Lett 17(3):1439–1447. https://doi.org/10.1021/acs.nanolett.6b04405

Hakalahti M, Faustini M, Boissière C et al (2017) Interfacial mechanisms of water vapor sorption into cellulose nanofibril films as revealed by quantitative models. Biomacromolecules 18(9):2951–2958. https://doi.org/10.1021/acs.biomac.7b00890

Hamedi MM, Hajian A, Fall AB et al (2014) Highly conducting, strong nanocomposites based on nanocellulose-assisted aqueous dispersions of single-wall carbon nanotubes. ACS Nano 8(3):2467–2476. https://doi.org/10.1021/nn4060368

Heise K, Kontturi E, Allahverdiyeva Y et al (2021) Nanocellulose: recent fundamental advances and emerging biological and biomimicking applications. Adv Mater 33(3):2004349. https://doi.org/10.1002/adma.202004349

Isogai A, Saito T, Fukuzumi H (2011) TEMPO-oxidized cellulose nanofibers. Nanoscale 3(1):71–85. https://doi.org/10.1039/C0NR00583E

Jacobs CB, Peairs MJ, Venton BJ (2010) Review: carbon nanotube based electrochemical sensors for biomolecules. Anal Chim Acta 662(2):105–127. https://doi.org/10.1016/j.aca.2010.01.009

Karunakaran C, Christensen CR, Gaillard C et al (2015) Introduction of Soft X-ray spectromicroscopy as an advanced technique for plant biopolymers research. PLoS One 10(3):e0122959. https://doi.org/10.1371/journal.pone.0122959

Kondor A, Santmarti A, Mautner A et al (2021) On the bet surface area of nanocellulose determined using volumetric, gravimetric and chromatographic adsorption methods. Front Chem Eng 3(September):1–12. https://doi.org/10.3389/fceng.2021.738995

Kontturi E, Laaksonen P, Linder MB et al (2018) Advanced materials through assembly of nanocelluloses. Adv Mater 30(24):1703779. https://doi.org/10.1002/adma.201703779

Kwon OH, Zewail AH (2010) 4D electron tomography. Science (80-) 328(5986):1668–1673. https://doi.org/10.1126/science.1190470

Laurila T, Protopopova V, Rhode S et al (2014) New electrochemically improved tetrahedral amorphous carbon films for biological applications. Diam Relat Mater 49:62–71. https://doi.org/10.1016/j.diamond.2014.08.007

Laurila T, Sainio S, Caro MA (2017) Hybrid carbon based nanomaterials for electrochemical detection of biomolecules. Prog Mater Sci 88:499–594. https://doi.org/10.1016/j.pmatsci.2017.04.012

Lawal AT (2016) Synthesis and utilization of carbon nanotubes for fabrication of electrochemical biosensors. Mater Res Bull 73:308–350. https://doi.org/10.1016/j.materresbull.2015.08.037

Leppänen E, Etula J, Engelhardt P et al (2021) Rapid industrial scale synthesis of robust carbon nanotube network electrodes for electroanalysis. J Electroanal Chem 896(January):115255. https://doi.org/10.1016/j.jelechem.2021.115255

Li Z, Wu Z, Li K (2009) The high dispersion of DNA-multiwalled carbon nanotubes and their properties. Anal Biochem 387(2):267–270. https://doi.org/10.1016/j.ab.2009.01.043

Li P, Sirviö JA, Hong S et al (2019) Preparation of flame-retardant lignin-containing wood nanofibers using a high-consistency mechano-chemical pretreatment. Chem Eng J 375(June):122050. https://doi.org/10.1016/j.cej.2019.122050

Li Y, Zhu H, Shen F et al (2015) Nanocellulose as green dispersant for two-dimensional energy materials. Nano Energy 13:346–354. https://doi.org/10.1016/j.nanoen.2015.02.015

Malho JM, Laaksonen P, Walther A et al (2012) Facile method for stiff, tough, and strong nanocomposites by direct exfoliation of multilayered graphene into native nanocellulose matrix. Biomacromolecules 13(4):1093–1099. https://doi.org/10.1021/bm2018189

Merkoçi A, Pumera M, Llopis X et al (2005) New materials for electrochemical sensing VI: carbon nanotubes. TrAC Trends Anal Chem 24(9):826–838. https://doi.org/10.1016/j.trac.2005.03.019

Muguruma H, Inoue Y, Inoue H et al (2016) Electrochemical study of dopamine at electrode fabricated by cellulose-assisted aqueous dispersion of long-length carbon nanotube. J Phys Chem C 120(22):12284–12292. https://doi.org/10.1021/acs.jpcc.6b03715

Niinivaara E, Faustini M, Tammelin T et al (2015) Water vapor uptake of ultrathin films of biologically derived nanocrystals: quantitative assessment with quartz crystal microbalance and spectroscopic ellipsometry. Langmuir 31(44):12170–12176. https://doi.org/10.1021/acs.langmuir.5b01763

Niinivaara E, Faustini M, Tammelin T et al (2016) Mimicking the humidity response of the plant cell wall by using two-dimensional systems: the critical role of amorphous and crystalline polysaccharides. Langmuir 32(8):2032–2040. https://doi.org/10.1021/acs.langmuir.5b04264

Oliveira T, Morais S (2018) New generation of electrochemical sensors based on multi-walled carbon nanotubes. Appl Sci 8(10):1925. https://doi.org/10.3390/app8101925

Olivier C, Moreau C, Bertoncini P et al (2012) Cellulose nanocrystal-assisted dispersion of luminescent single-walled carbon nanotubes for layer-by-layer assembled hybrid thin films. Langmuir 28(34):12463–12471. https://doi.org/10.1021/la302077a

Ortolani TS, Pereira TS, Assumpção MH et al (2019) Electrochemical sensing of purines guanine and adenine using single-walled carbon nanohorns and nanocellulose. Electrochim Acta 298:893–900. https://doi.org/10.1016/j.electacta.2018.12.114

Osorio A, Silveira I, Bueno V et al (2008) H2SO4/HNO3/HCl-functionalization and its effect on dispersion of carbon nanotubes in aqueous media. Appl Surf Sci 255(5):2485–2489. https://doi.org/10.1016/j.apsusc.2008.07.144

Osorio DA, Seifried B, Moquin P et al (2018) Morphology of cross-linked cellulose nanocrystal aerogels: cryo-templating versus pressurized gas expansion processing. J Mater Sci 53(13):9842–9860. https://doi.org/10.1007/s10853-018-2235-2

Palomäki T, Peltola E, Sainio S et al (2018) Unmodified and multi-walled carbon nanotube modified tetrahedral amorphous carbon (ta-C) films as in vivo sensor materials for sensitive and selective detection of dopamine. Biosens Bioelectron 118(July):23–30. https://doi.org/10.1016/j.bios.2018.07.018

Papakonstantinou P, Kern R, Robinson L et al (2005) Fundamental electrochemical properties of carbon nanotube electrodes. Fullerenes Nanotub Carbon Nanostruct 13(2):91–108. https://doi.org/10.1081/FST-200050684

Peltola E, Wester N, Holt KB et al (2017) Nanodiamonds on tetrahedral amorphous carbon significantly enhance dopamine detection and cell viability. Biosens Bioelectron 88:273–282. https://doi.org/10.1016/j.bios.2016.08.055

Primo E, Gutierrez F, Luque G et al (2013) Comparative study of the electrochemical behavior and analytical applications of (bio)sensing platforms based on the use of multi-walled carbon nanotubes dispersed in different polymers. Anal Chim Acta 805:19–35. https://doi.org/10.1016/j.aca.2013.10.039

Protopopova V, Iyer A, Wester N et al (2015) Ultrathin undoped tetrahedral amorphous carbon films: The role of the underlying titanium layer on the electronic structure. Diam Relat Mater 57:43–52. https://doi.org/10.1016/j.diamond.2015.06.009

Rastogi R, Kaushal R, Tripathi S et al (2008) Comparative study of carbon nanotube dispersion using surfactants. J Colloid Interface Sci 328(2):421–428. https://doi.org/10.1016/j.jcis.2008.09.015

Rossell MD, Kuebel C, Ilari G et al (2013) Impact of sonication pretreatment on carbon nanotubes: a transmission electron microscopy study. Carbon 61:404–411. https://doi.org/10.1016/j.carbon.2013.05.024

Sainio S, Wester N, Aarva A et al (2021) Trends in carbon, oxygen, and nitrogen core in the X-ray absorption spectroscopy of carbon nanomaterials: a guide for the perplexed. J Phys Chem C 125(1):973–988. https://doi.org/10.1021/acs.jpcc.0c08597

Saito T, Kimura S, Nishiyama Y et al (2007) Cellulose nanofibers prepared by TEMPO-mediated oxidation of native cellulose. Biomacromolecules 8(8):2485–2491. https://doi.org/10.1021/bm0703970

Shahrokhian S, Naderi L, Ghalkhani M (2015) Nanocellulose/carbon nanoparticles nanocomposite film modified electrode for durable and sensitive electrochemical determination of metoclopramide. Electroanalysis 27(1):2637–2644. https://doi.org/10.1002/elan.201500266

Shalauddin M, Akhter S, Basirun WJ et al (2019) Hybrid nanocellulose/f-MWCNTs nanocomposite for the electrochemical sensing of diclofenac sodium in pharmaceutical drugs and biological fluids. Electrochim Acta

304:323–333. https://doi.org/10.1016/j.electacta.2019.03.003

Sirviö JA, Ukkola J, Liimatainen H (2019) Direct sulfation of cellulose fibers using a reactive deep eutectic solvent to produce highly charged cellulose nanofibers. Cellulose 26(4):2303–2316. https://doi.org/10.1007/s10570-019-02257-8

Tang Y, Yang H, Vignolini S (2022) Recent progress in production methods for cellulose nanocrystals: leading to more sustainable processes. Adv Sustain Syst. https://doi.org/10.1002/adsu.202100100

Tessonnier JP, Ersen O, Weinberg G et al (2009) Selective deposition of metal nanoparticles inside or outside multiwalled carbon nanotubes. ACS Nano 3(8):2081–2089. https://doi.org/10.1021/nn900647q

Tong X, Liu M, Zhao G (2010) Construction of a carbon nanotube/diamond hybrid functionalized electrode surface. J Solid State Electrochem 14(2):221–224. https://doi.org/10.1007/s10008-009-0837-y

Tsierkezos NG, Othman SH, Ritter U et al (2016) Electrochemical analysis of ascorbic acid, dopamine, and uric acid on nobel metal modified nitrogen-doped carbon nanotubes. Sens Actuators B Chem 231:218–229. https://doi.org/10.1016/j.snb.2016.03.032

Vashist SK, Zheng D, Al-Rubeaan K et al (2011) Advances in carbon nanotube based electrochemical sensors for bioanalytical applications. Biotechnol Adv 29(2):169–188. https://doi.org/10.1016/j.biotechadv.2010.10.002

Wang H, Biswas SK, Zhu S et al (2020) Self-healable electro-conductive hydrogels based on core-shell structured nanocellulose/carbon nanotubes hybrids for use as flexible supercapacitors. Nanomaterials 10(1):112. https://doi.org/10.3390/nano10010112

Wester N, Sainio S, Palomäki T et al (2017) Partially reduced graphene oxide modified tetrahedral amorphous carbon thin-film electrodes as a platform for nanomolar detection of dopamine. J Phys Chem C 121(14):8153–8164. https://doi.org/10.1021/acs.jpcc.6b13019

Yu J, Grossiord N, Koning CE et al (2007) Controlling the dispersion of multi-wall carbon nanotubes in aqueous surfactant solution. Carbon 45(3):618–623. https://doi.org/10.1016/j.carbon.2006.10.010

Zaid MHM, Abdullah J, Yusof NA et al (2020) Reduced graphene oxide/TEMPO-nanocellulose nanohybrid-based electrochemical biosensor for the determination of mycobacterium tuberculosis. J Sensors 2020:1–11. https://doi.org/10.1155/2020/4051474

Zhang Y, Nypelö T, Salas C et al (2013) Cellulose nanofibrils. J Renew Mater 1(3):195–211. https://doi.org/10.7569/JRM.2013.634115